OPTICAL EMISSION CHARACTERIZATION OF HIGH-POWER HALL THRUSTER WEAR

George J. Williams, Jr.
The Ohio Aerospace Institute
NASA Glenn Research Center
Cleveland, OH

Hani Kamhawi
NASA Glenn Research Center
Cleveland, OH

ABSTRACT

Optical emission spectroscopy is employed to correlate BN insulator erosion with high-power operation of the NASA 300M Hall-effect thruster. Actinometry leveraging excited xenon states is used to normalize the emission spectra of ground state boron as a function of thruster operating condition. Trends in the strength of the boron signal are correlated with thruster power, discharge voltage, discharge current and magnetic field strength. The boron signals are shown to trend with discharge current and show weak dependence on discharge voltage. The trends are consistent with data previously collected on the NASA 300M and NASA 457M thrusters but are different from conventional wisdom.

NOMENCLATURE

$I_{A,\lambda}$ = Intensity of a transition of species A at wavelength, λ.
J_D = Discharge, current, A
N_B = normalized signal strength for the boron transition
S = Amplification factor
$T(\lambda)$ = Optical transmission function
V_D = discharge voltage, V
z/Wc = Axial position normalized by channel width

INTRODUCTION

NASA's Hall-effect thrusters (HETs) are being designed to higher fidelity to support near term missions. In general, demonstration of thruster performance is straightforward and correlation of performance anomalies to design trades can be accomplished via standard physical probes located in the far to mid-plume plasma. However, life-assessment and the impacts small modifications have on the near-field plasma require near field measurements which are very difficult with physical probes. Optical diagnostics offer the potential to make non-intrusive measurements but often indirectly measure the plasma properties requiring simplifying assumptions or rigorous numerical modeling.

Hall thrusters are a type of electric propulsion (EP) thruster with performance that is well suited for a number of future NASA space missions. Low power (< 1 kW) Hall thrusters enhance and enable a number of small body and Radioisotope-driven Electric Propulsion (REP) class science missions. Medium power (~3.5-4.5 kW) Hall thrusters enhance and enable many NASA Discovery and New Frontier class science missions, while 4.5-10kW EP systems would be most applicable to NASA New Frontiers and Flagship class missions. High power (>20kW) EP systems are enabling and enhancing for time critical missions or missions requiring transportation of large payloads. A number of mission studies were performed highlighting the enhancing and enabling features of high power EP systems for reusable space tug applications for the transfer of payloads from LEO to GEO and for use in Mars mission scenarios.[1,2,3]

Several investigations have used optical emission spectroscopy (OES) to characterize the erosion of the Boron-Nitride (BN) insulators in HETs.[4,5,6,7,8,9,10,11,12] Quantifying the extent to which the OES signal represents the erosion rate remains the greatest challenge to OES as an erosion diagnostic. Emission signals are integrated over collection volumes and generally this leads to a lack of spatial resolution and to the possibility of detecting the same particles multiple times depending on sputter rate and plasma conditions. To some extent this can be mitigated through the use of spatial filters and multiple collection volumes. Even if the monitored transition is a ground-state transition of the sputtered material, the signal strength is proportional not only to the number density of the species, but also to the excitation rate of the sputtered atoms which is a function of the local plasma. As discussed below, electron excitation cross-sections of boron and other materials of interest to life assessment of electric propulsion systems are largely unknown. Moreover, even if these cross-sections are known, the electron temperatures in the regions of interest are extremely difficult to measure and are largely inferred from models. This precludes even the application of simple corona models to evaluate the relative signal strengths. In addition, sputtered atoms are excited to a number of states. Most of these are transitions to and from the ground state, and several different techniques have been proposed to correlate the number of atoms excited to one particular state to the total number of sputtered atoms.[13] Finally, even if this correlation can be resolved through an analysis of the relative excitation cross-sections, the diffuse nature of the sputtered material makes determination of the very local erosion rate via OES appear nearly impossible to determine.

An approach incorporating actinometry was developed by Pagnon[6] and implemented previously in the characterization of several NASA HETs.[14] Actinometry uses the emission of one species (which is well-characterized) to correct the emission of another and is limited to applications with corona equilibrium and to where the species have similar cross-sections, thresholds, and shapes as a function of electron energy.[15] That investigation showed that normalizing the emission of boron atoms through actinometry captured trends in the emission with operating condition. However, the trends suggested that insulator erosion was primarily a function of discharge current and not discharge voltage, as is conventionally assumed. Preliminary results of recent numerical modeling have confirmed the possibility of this dependence.[16] Nevertheless, the investigation did not validate the OES techniques ability to measure even relative erosion rates. False trends yielded by iron spectra masking the emission of boron atoms was another concern.

The current investigation at NASA GRC was intended to address these questions and advance the confidence in the technique. A multi-layer foil sample was incorporated in the near-field plume of the NASA 300M to provide a validation mechanism for absolute erosion measurements. Unfortunately, the results of this aspect of the investigation were inconclusive as the layers of the foil appeared to erode simultaneously instead of sequentially. However, incorporation of lessons learned in the collection and analysis of the emission spectra were coupled with the measurement of near-infrared spectra to improve the quality of the measurements. Data were collected to validate the trends observed in previous testing and to address the possible contamination of the data by Fe emission. If these can be addressed satisfactorily, the technique will remain useful for model validation and the ongoing STMD development of a 10 to 15 kW HET. These results are discussed at length below.

EXPERIMENTAL HARDWARE

NASA 300M HALL EFFECT THRUSTER

The NASA-300M was designed and fabricated under the support of the ESMD Exploration System Research and Technology (ESR&T) Program in 2005. The NASA-300M design is a scaled version of the NASA-457Mv2.[17] The NASA-300M design incorporated lessons learned from the development and testing of the NASA-457M, NASA-400M, and NASA-457Mv2 thrusters. The goal of the design was to minimize thruster size while optimizing the magnetic field and plasma lens to attain improved performance. The NASA-300M nominal design specifications

were a discharge power of 20 kW, a discharge voltage range of up to 600 V, a discharge current of up to 50 A, and a magnetic circuit that has a magnetic field topology similar to the NASA-457Mv2. At 20 kW the thruster produced a peak thrust of 1.13 N, a peak total thrust efficiency of ~67% was achieved at a discharge voltage of 400 V and a peak total specific impulse of 2,916 s was demonstrated at a discharge voltage of 600 V.[17]

The 300M was operated in Vacuum Facility 5 (VF5) at NASA GRC. VF 5 utilized a combination of diffusion pumps and cryo surfaces to maintain a pressure near the thruster less than $3 \cdot 10^{-5}$ Torr (corrected for Xe) during full power operation of the thruster. The operation leveraged a laboratory propellant feed system and power console, an inverted pendulum thruster stand, a data acquisition system, and several physical probes for plume interrogation. Detailed discussion of the testing of the 300M is available in a paper of Herman[18]. Far field plume analyses are provided in a companion paper by Huang.[19]

Figure 1 shows a photograph of the 300M in VF-5 with optical probes mounted above the thruster. The thruster was operated near the centerline of the chamber for most of the data presented below. However, the thruster was on a translation stage which could move the thruster while operating to one side for high-speed physical probe measurements (to be published in an upcoming paper by Shastry) and to the other side for interrogation by an upstream-facing optical probe. The optical probes mounted above the thruster moved with the thruster.

OPTICAL PROBES

Optical probes were constructed using 2.5 cm diameter UV-silica lenses and flat windows, optical tubes, and SMA fiber optic connections. Lenses which matched the acceptance angle of the 400 μm diameter UV-VIS fiber optic cables and protective windows were incorporated in all of the probes. A second lens with a 30 cm focal length was incorporated in a threaded section which allowed adjustment of the focal point. Single-fiber, 400 μm core diameter, metal-jacketed fiber optic cables coupled the probes to vacuum feed thrus and the feed thrus to a fiber optic multiplexer located external to the vacuum chamber. The probes were mounted near the thruster outside of a 45-degree exclusion zone. Similar fiber optic cables connected the feed-thrus to an optical multiplexer which switched the signals from each probe through each of three spectrometers. The digital spectrometers measured emission in the 220-420 nm, 480-540 nm and 780 to 900 nm regions.

Figure 1 also shows the arrangement nominal configuration of the probes with respect to the thruster and the zone of interrogation on the inner wall of the BN insulator. Measurements were taken in two test segments. In the first, data were collected from three probes focused on the erosion zone of the outer wall of the BN insulator. In the second segment, shown schematically to the right in Fig. 1, three probes were focused on the erosion zone of the inner wall of the BN insulator and one was focused on the outer wall. The fourth probe was left unaltered from the first segment of testing to provide a correlation between the inner and outer wall emission signals. Assuming that the thruster will operate and erode in a repeatable fashion at the same operating conditions over these short test segments, the fourth probe directly accounts for probe degradation due to sputter coating and to slight differences in operating conditions.

These probes were mounted to the thruster mount which moved with the thruster as it was translated to support rapid axial probe measurements. Another probe was mounted in a fixed position downstream of the thruster. This probe was typically out of the thruster plume, but the thruster was translated to obtain spectra looking upstream through the plume. The goals of these measurements were to identify a distance from the inner or outer BN wall in which the B emission signal disappeared and to identify Fe transitions which should be maximized on the centerline of the discharge channel. A quartz window thermally isolated from the collection optics was placed in front of this axial probe.

The transmission through the probes was calibrated before, during, and after each test. Standard Xe and W lamps were placed at the same distance as the location of measurement in the thruster for each probe and spectral data were recorded using the entirety of the probe-fiber-feed thru system before and after each series of testing. Minor variations were noted which were likely the result of sputter deposition on the protective windows. The deposition tended to preferentially reduce the signal strength below a wavelength of 350 nm. However, the degradation was negligible. Calibrations were performed during a test sequence by recording spectra at repeated thruster operating conditions. No significant changes in line intensities were noted, and the slight degradation of the UV signal was recorded and used in the normalization of the data.

THEORY

In order to correlate the observed spectra to physical characteristics of the plasma and the erosion, it is necessary to relate the changes in the strengths of particular transitions to changes in the species or in plasma as a whole. One method to accomplish this is to develop a comprehensive collisional-radiative (CR) model of excitation and de-excitation processes of the electronic state transitions yielding the observed emission spectra. For example, Cho has done this for several near-infrared transitions in neutral xenon. No CR model has been developed for boron. Since the ground state transition couplet of B I at 249.68 nm and 249.77 nm is populated almost exclusively by electron impact and depopulated by spontaneous emission, a corona model is justified. However, the excitation cross-section is unknown. Pagnon demonstrated that one can approximate the cross-section using actinometry to normalize the B OES signals.[6] Actinometry uses the emission of one species (which is well-characterized) to correct the emission of another and is limited to applications with corona equilibrium and where the species have similar cross-sections, thresholds, and shapes as a function of electron energy.[15]

Following Pagnon,[6] the upper state $5p^1D^0$ (7/2) of the Xe II (484 nm) is populated principally by radiative decay from two ionic metastable states $5d^1D$ (7/2) and $5d^1F$ (7/2). Therefore, the electrons that excite the 484 nm line (via the metastable states) have similar energy to those that excite the 250 nm boron line. The excitation of the two states should vary similarly with changes in the discharge. However, being an ion transition, the degree of ionization must also be accounted for. Pagnon does this by including the strength of the Xe I (828 nm) transition which is also included in this investigation. All means of excitation including ion-atom collisions are included in this way—there is no need to separate them into specific rate coefficients. The resulting expression for the amount of sputtered material, N_B, is

$$N_B \propto \frac{I_{B,\ 250\ nm} \cdot I_{Xe\ I,\ 828\ nm}}{I_{Xe\ II\ 484\ nm}} \tag{1}$$

If N_B at a particular operating condition can be tied to an insulator erosion rate, then Eq 1 can be used to predict the erosion at other operating conditions.

Before the intensities of the lines were included in Eq 1 or any other comparative analysis, the raw signals were corrected for systematic perturbations or errors. These include offsets in the spectrometer baseline, transmission losses, and amplification through spectrometer sensitivity settings or data logging software. Equation 2 summarizes the correction of each raw signal:

$$I_\lambda^{cor} = \left(\frac{I^{raw} - I^{offset}}{S} \right) T(\lambda) \tag{2}$$

,

where $T(\lambda)$ is a self-normalized transmission function unique to each probe and S is an amplification correction factor unique to each wavelength. Since no "raw" data are presented, the superscript "raw" is dropped throughout this paper. "Uncorrected" data are those which have not undergone the normalization of Eq 1.

RESULTS AND DISCUSSION

OVERVIEW OF OES SIGNALS

The emission spectra of boron is limited to a few accessible transitions within a sea of xenon transitions (especially Xe II and Xe III). However, iron also has emission in the same region with more spectral lines than xenon. Sources of sputtered iron include the anode and stainless probes or mounts near the thruster. Figure 2a shows the wavelength and relative intensities of Xe II, Xe III, Fe I, Fe II, and B I transitions in the 247 nm to 252 nm region. (There are no Xe I or B II transitions in this region and only one Fe II transition at 248.81 nm.) Note the proximity of the Fe I transition at 249.65 nm to the boron transitions.

Figure 2b overlays a typical emission spectrum acquired looking across the plume of the 300M 5 mm downstream of the thruster exit plane in a previous test sequence.[14] Note that the peaks in the spectrum correspond to Xe II (and perhaps Xe III) transitions. There is no evidence of B or Fe spectra. Figure 2c overlays typical emission spectra at V_D = 300 V, J_D = 40 A. The cross-plume spectra from Fig. 2b is shown with that of a probe focused on the inner wall at z/W_C = 0.1 and with that of a collimated probe centered in the discharge channel looking upstream towards the anode. Note that the signals from the probe focused on the wall and the probe across the plume lie on top of each other except for the region of the B transitions. (Slight differences in the Xe profiles result from slight differences in the probe configuration and quality and possibly from slight differences in thruster operating condition.) However, several small features are present in the axial spectra (the red trace with open-circle markers) indicating the presence of Fe atoms. These are noted in the Figure. The emission around 250 nm associated with the Fe emission is broad and multi-peaked resulting from a convolution of the Fe and B emission. Without Fe emission, the B signal is narrower and peaked closer to 250 nm.

The only spectra which show evidence of Fe emission are those from the probe looking axially upstream into the discharge. All of the spectra used to evaluate the BN erosion show only the B transitions near 250 nm and none of the other Fe-spectral features (e.g. near 248.5 nm and 252 nm). This indicates that the data from the probes focused on the channel walls are free of contamination from Fe emission.

Unfortunately, the axial probe did not resolve a clean transition from B-to-Fe-to-B emission across the channel as the thruster was translated in front of it. This is partially because the probes collection cross-section, about 1 cm^2, simultaneously observed significant regions of the anode and downstream BN surfaces and partially because the signals of both Fe and B were so small that large integration times were required to resolve their spectra in the presence of the very large Xe background signal. The dwell time of the thruster in front of the probe associated with the latter was deemed too detrimental to both the thruster and the probe.

Figure 3 compares the corrected $I_{B,\,250\ nm}$ signal with that of N_B at discharge voltages of 300 V and 400 V as a function of discharge current. The curves are normalized to the maximum N_B and $I_{B,\,250\ nm}$ values. These coincide at 300 V, 50 A which may have been an anomalous point as discussed below. The trends in Fig. 3 indicate that the actinometry reduces the sensitivity of the signal, but that it does not significantly alter the trends from the non-normalized emission data. This is consistent with previous data.[14]

OES MEASUREMENT OF SPUTTER-ERODED BORON

Optical emission spectra were collected over a wide range of thruster operating conditions. However, most of the data were collected at a discharge voltage of 300 V. Tens of minutes passed between the establishment of an operating point and the collection of OES data. Magnet current settings were optimized for each operating point and/or set to values consistent with previous thruster performance testing. Since OES data were collected on the inner and outer walls during different testing segments, data at the same operating condition are not always available. In particular, the test segment during which inner wall OES data were collected was much shorter than that in which outer wall OES data were collected. As described above, OES data were collected from one location of outer wall to facilitate correlating the two sets of data.

For the sake of discussion, the trends observed in N_B values are assumed to represent trends in the amount of B sputtered locally from the BN. A multi-layer foil in-situ measurement proved inconclusive with respect to validating an erosion rate measurement. The sample incorporated lessons learned during a previous measurement,[14] but instead of yielding clear transitions between Au and Ag emission, both were observed from the outset in mirror-image trends. The technique has been validated in previous investigations with coupons that used BN layers to quantify the erosion and metal foils to simply signal the transition from one to the other layer of BN.[11] While the N_B trends reported here are consistent with previous OES data and to recent preliminary modeling efforts, further validation is required. This validation may take the form of coupons or of wear tests of moderate duration, e.g. 100's of hours in duration. In the latter, laser profilometry could be used to validate the OES erosion-predictive capability. This option appears more promising given the little contamination and degradation of the optical probes by back-sputtered material in these recent performance tests.

Uncertainty in the values of N_B results from the signal to noise ratios of $I_{B,250\ nm}$, $I_{Xe\ 828\ nm}$ and $I_{Xe+,\ 484\ nm}$, the degree to which these lines fulfill the actinometry function, alignment, and contamination of the optics. For low levels of $I_{B,\ 250}$ the signal to noise ratios could be as low as 2. However, by removing background and dark currents and digitally averaging the spectra before recording the intensity values, the ratios were increased to around 10 for most of the data, yielding a ±10% uncertainty. $I_{Xe+,\ 484\ nm}$ and $I_{Xe,\ 828\ nm}$ were much cleaner with repeatability within 1%. Pre- and post-test calibration of the optics showed very little degradation from coating. Use of $I_{Xe,\ 828\ nm}$ instead of $I_{Xe,\ 407\ nm}$ significantly improved the signal to noise of the actinometry variables as well as bringing these measurements in line with common practice and previous validation.[6] To capture the uncertainties in the OES signal strengths, an uncertainty of ±10% should be assumed for all N_B values given below. At this time, quantifying the uncertainty in how well the actinometry is accounting for changes in the electron temperature is not possible.

Figure 4 shows trends in N_B at three locations on the inner insulator wall for discharge voltages of 300 V and 400 V over a range of currents. Note that there is a much stronger dependence on J_D at 300 V than at 400 V. This is consistent with previous OES data obtained on the NASA 457M thruster and may result from the acceleration zone being either extended axially across this region at 400 V or from the acceleration zone being largely downstream of the exit plane at 400 V. High-speed probe data should provide more insight into this phenomenon. The data in both Fig. 4a and Fig. 4b are normalized to the maximum value of the combined data set. The N_B values are very similar for the two sets of data between discharge currents of 20 A and 40 A. No data were collected at 400 V, 50 A so whether the trends would sharply increase at 50 A is unknown, though this would be consistent with previous data. Note also that the N_B values at the upstream end of the erosion zone, $z/W_C = 0.20$, are trending higher at low J_D for the $V_D = 400$ V case which suggests that the high-density and/or high-temperature plasma region is further upstream for the higher-voltage case.

Figure 5 compares trends in N_B for discharge currents of 40 A and 25 A at the same three axial locations for several discharge voltages. The N_B values are normalized to the same

value as they were in Fig. 4. Data associated with z/W_C = 0.1 and 0.2 are very weakly increasing with V_D. Either the ions impacting the BN in this region are not increasing significantly in energy or the number of impacting ions is significantly being reduced. Near the exit plane, the N_B signal increases significantly as V_D increases above 400 V. This suggests that the eroding ions are gaining energy, are diverging more into the wall, or are simply increasing in number. While none of these would be surprising, the lack of such a trend for V_D < 400 V is surprising.

Figure 6a shows increasing N_B values with increasing discharge current along the outer wall of the BN insulator for V_D = 300 V. Multiple N_B values resulted at some J_D due to variations in the operating conditions, duration of thruster operation prior to collection of OES data (particular to that point and cumulative), and uncertainty in the OES technique itself. (Trendlines are provided for ease in reading the graph and are not an attempt to suggest an actual dependence.) N_B values in Fig. 6a and 6b are normalized together as a set of outer-wall data. Figure 6b shows a weak dependence of N_B on discharge voltage for J_D = 40 A which is similar to the dependence of the z/W_C values of 0.1 and 0.2 of Figs. 5a and 5b.

Figure 7 correlates the N_B trends observed on the inner wall and outer wall at the z/Wc = 0.10 location. The data are normalized to the maximum of all three sets of data. No other scaling was required to achieve agreement between the outer wall data taken previously to and simultaneously with the inner wall data for all operating conditions with J_D < 50 A. This validates test-to-test repeatability of the technique and the ability to correlate OES data from different test segments. In addition, the inner wall and outer wall data agree for these points. However, at J_D = 50 A there is a significant divergence: the inner wall values increase more rapidly than a linear trend would suggest (as best seen in Fig. 4a) and the outer wall N_D values increase even more. However, the previous outer wall values appear to roll over at J_D = 40 A. The two 15 kW operating points (one yielding green and red data and the other the blue data) differ only in anode mass flow rates. The flow rate associated with the higher N_B values is about 5% less than the one associated with the lower N_B values. A lower flow rate associated with the same discharge current suggests a less efficient discharge. A previous correlation of N_B with anode efficiency showed that lower efficiencies yielded higher N_B. Since no thrust data were collected during the current set of tests, a similar analysis cannot be completed with these data, but these few points appear to qualitatively show that trend. Neglecting the points at a J_D = 50 A, the data suggest that the inner and outer walls erode at the same rate at z/Wc = 0.1. Similar agreement is seen at z/Wc = 0.20.

Figure 8 compares the trends in N_B for the locations closest to the exit plane on the inner and outer walls for V_D = 300 V operation. For all J_D, the inner wall appears to have a slightly higher erosion rate which is consistent with previous data. Note, however, there is no change in the trend of the inner wall data at the J_D = 50 A point of operation. Therefore, if the flow rate difference between the two sets of data shown in Figs. 7 and 8 at J_D = 50 A were the cause of the jump in Fig. 7, it would have had resulted in either increasing the divergence of the beam or of bringing the acceleration zone further upstream, or both.

Modest (~ 10%) variations in the magnet coil currents resulted in proportional changes in the N_B values. In general, as the inner magnet current was increased, the inner N_B value decreased. The same relationship was observed between the outer magnet current and the outer N_B values. If both were increased, both N_B decreased and if both currents decreased, both N_B increased. These trends were observed over the entirety of the testing, but unequal settings of the magnet currents often were associated with weak plasma instabilities or hot spots as the thruster power was increased. During previous testing of the NASA 457M, it was observed that large changes (300%) in the magnet currents yielded significantly higher N_B values. With caveats, by capturing these trends the OES technique may prove helpful in optimizing the magnet current settings by correlating the performance with insulator erosion.

SUMMARY AND CONCLUSIONS

Fiber optic probes characterized the relative erosion of the BN insulator of the NASA 300M HET. The emission of boron atoms has been normalized using an actinometrical method that mitigates the need to know the electron temperature in the discharge or the detailed excitation and quenching mechanisms of the B I transitions. The technique yielded a real-time, non-intrusive diagnostic that captured trends in BN insulator erosion assuming that the amount of sputtered B atoms is proportional to the BN erosion rate and that the N_B values are proportional to the amount of sputtered B atoms. Both of these remain to be validated. In this regard, it remains appropriate to refer to the trends as trends in N_B and not in erosion rates.

The technique demonstrated the ability to provide real-time relative assessment of the impact of changes in the operating conditions on N_B. Also, the clear differences in $I_{B,250}$ collected from probes focused a few millimeters apart on the BN walls demonstrated the ability to measure N_B with spatial resolutions on the order of a few millimeters within the thruster. As in a previous investigation, N_B was primarily a function of discharge current and not discharge voltage. Small changes in magnet currents also resulted in changes in N_B and this may support the definition of optimal thruster operating conditions and the impact of operating slightly off-nominal conditions. Near the exit plane, the inner wall of this thruster had higher N_B values than the outer wall. However, a few millimeters further upstream, the inner and outer walls appear to yield the same N_B values and trends.

This investigation validated the test-to-test repeatability and correlation of the OES technique. Not only was no scaling required to correlate spectra from two different test segments, trends observed in testing of the same thruster several months apart were nearly identical for identical operating conditions. For slightly different operating conditions, changes in the N_B values correlated with thruster efficiencies. Also, this investigation mitigates the concern that Fe emission precludes the collection of useful data. It did show, however, that spectra collected from axial-looking probes will require deconvolution of Fe and B spectra.

The OES technique which leverages actinometry remains promising. However, validation of the technique's ability to measure erosion and not just N_B remains a high priority. Multilayer coupons which use metal foils as erosion measures has proven inconclusive and potentially disruptive to thruster testing. However, metal foil indicators as the transition between thin layers of BN remains a possible approach. As HET development continues, moderate duration (100's of hours) wear tests may prove an effective validation mechanism. This is supported by the lack of degradation of the optical probes during extended performance testing. Results of recent internal electrostatic probe measurements and advances in numerical modeling (anchored to these measurements) will be correlated with the N_B trends. While not providing validation or refutation, agreement and consistency will add to the confidence of using this technique.

ACKNOWLEDGMENTS

The authors would like to thank and acknowledge the Office of the Chief Technologist for funding this work as well as Timothy Smith for serving as the Project Manager. The authors also thank Kevin McCormick for his aid in fabricating the metallic coupons used in this study and George Readus, George Jacynycz and Kevin Blake for maintaining and operating the vacuum facilities.

REFERENCES

[1] Dudzinski, L., et al., "Design of Solar Electric Propulsion Transfer Vehicle for a Non-Nuclear Human Mars Exploration Architecture," 26th International Electric Propulsion Conference Paper IEPC-99-181, Japan, October 1999.

[2] Oleson, S.R., "Advanced Propulsion for Space Solar Power Satellites," 35th AIAA Joint Propulsion Conference, AIAA-99-2872, Los Angeles, California, June 1999.

[3] Oleson, S.R., et al., "Mission Advantages of Constant Power Variable Specific Impulse Electrostatic Thrusters," NASA TM-2000-210477, 2000.

[4] Leray, P., *et al.,* "Spatially Resolved Emission Spectroscopy Along a SPT Channel, Interpretation of Data by a Collisional-Radiative Model," International Electric Propulsion Conference Paper IEPC-97-054, Cleveland, Ohio 1997

[5] Karabadzhak, G. F., and Semenkin, A. V., "Investigation of TAL Optical Emissions," International Electric Propulsion Conference Paper IEPC-97-131, Cleveland, Ohio, 1997.

[6] Pagnon, D., Touzeau, M., and Lasgorceix, P., "Control of the Ceramic Erosion by Optical Emission Spectroscopy: Parametric Studies of SPT 100-ML," AIAA Paper 2004-3773, July 2004.

[7] Hargus, W. A., "Optical Boron Nitride Insulator erosion Characterization of a 200 W Xenon Hall Thruster," 41st AIAA Joint Propulsion Conference, AIAA paper 2005-3529, Tucson, Arizona, 2005.

[8] Cho, S., *et al.,* "Experimental and Numerical Study on a Hall Thruster Insulator Erosion," International Electric Propulsion Conference Paper IEPC-2011-078, Wiesbaden, Germany, September 2011.

[9] Shmelev, A. V., and Lovtsov, A., S., "Investigation of Discharge Power Influence on Erosion Rate of SPT Discharge Chamber Using Spectroscopic Method," International Electric Propulsion Conference Paper IEPC-2011-024, Wiesbaden, Germany, September 2011

[10] Kozintseva, M. V., *et al.,* "Forecast of Erosion Rate of SPT K-0 Channel Insulators by Spectral Measurements," International Electric Propulsion Conference Paper IEPC-2011-293, Wiesbaden, Germany, September 2011.

[11] Cho, S., *et al.,* "Hall Thruster Channel Wall Erosion Rate Measurement Method Using Multilayer Coating Chip," 46th AIAA Joint Propulsion Conference, AIAA-2010-6697, Nashville, Tennessee, July 2010.

[12] Arabadzhak, G. F. and Semenkin, A. V., "Evaluation of a Xenon Operating Hall Thruster Body Erosion Rate Through Analysis of Its Optical Spectra," 37th AIAA Joint Propulsion Conference, AIAA-2001-3889, Salt Lake City, Utah, July 2001.

[13] Chiu, Y. H., et al., "Passive Optical Diagnostic of Xe Propelled Hall Thrusters, Part 1: Emission Cross Sections, *Journal of Applied Physics* **99** 113304 (2006).

[14] Williams, G. J., Soulas, G. C., and Kamhawi, H., "Optical Daignsotic Characteriation of High-Power Hall Thruster Wear and Operation," 48th AIAA/ASME/SAE/ASEE Joint Propulsion Conference, AIAA Paper 2012-4036, Atlanta, GA, July, 2012.

[15] Selwyn, G. S., Optical Diagnostic Techniques for Plasma Processing, American Vacuum Society, New York, 1993, pp47-50.

[16] Mikellides, I. G., Senior Researcher, NASA JPL, Personal Communication, October, 2012.

[17] Kamhawi, Hani, et al., "Overview of Hall Thruster Activities at NASA Glenn Research Center," International Electric Propulsion conference Paper IEPC-2011-339, Wiesbaden, Germany, 2011.

[18] Herman, D. A., Shastry, R., Huang, W., Soulas, G. C., and Kamhawi, H., "Plasma Potential and Langmuir Probe Measurements in the Near-field Plume of the NASA 300M Hall Thruster," Presented at the 48th AIAA/ASME/SAE/ASEE Joint Propulsion Conference, AIAA Paper 20012-4196, Atlanta, GA, July, 2012.

[19] Huang, W., Shastry, R., Soulas, G., and Kamhawi, H., "Farfield Plume Measurement and Analysis on the NASA-300M," 60th JANNAF Propulsion Meeting, Colorado Springs, CO, April 29 - May 3, 2013.

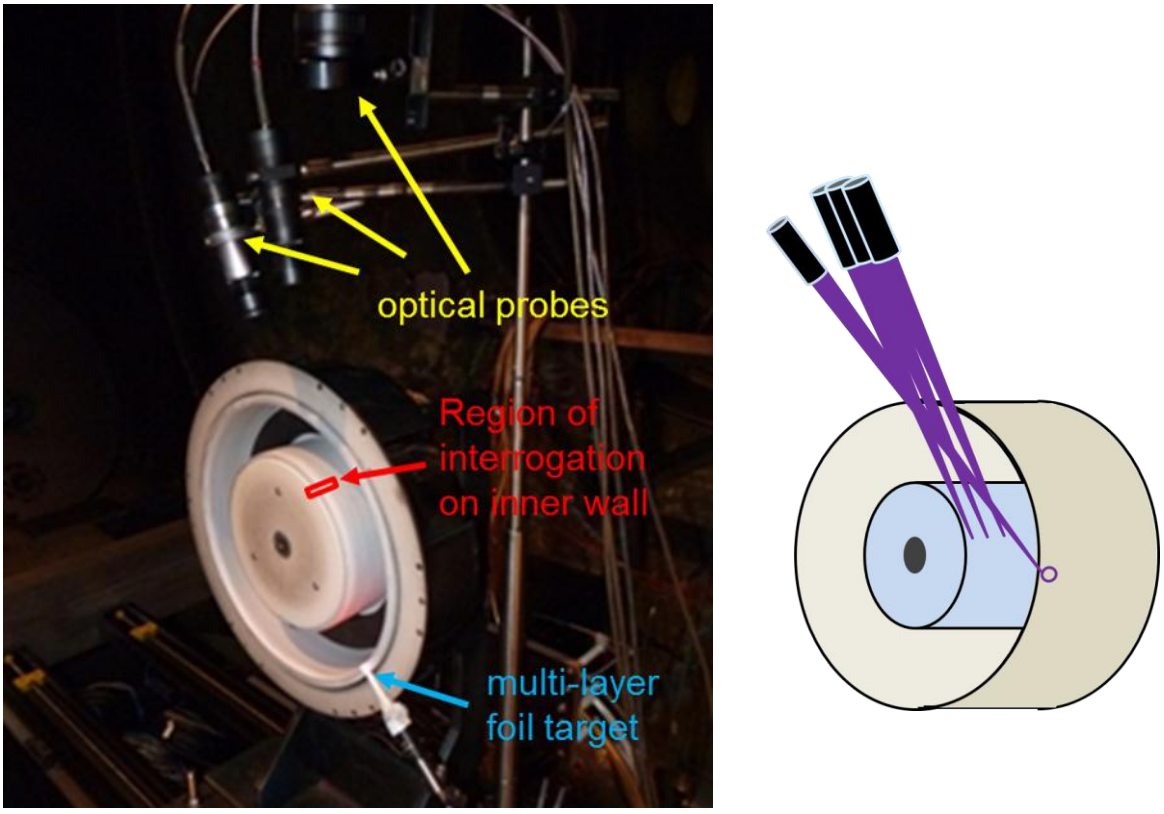

Figure 1 Photograph of the NASA 300M and showing optical probes above the thruster, the nominal region of interrogation on the inner wall of the BN insulator, and the multi-layer foil target at the 5 o'clock position of the thruster The schematic on the right shows the relative locations of the interrogation points for the three inner wall probes and one outer wall probe.

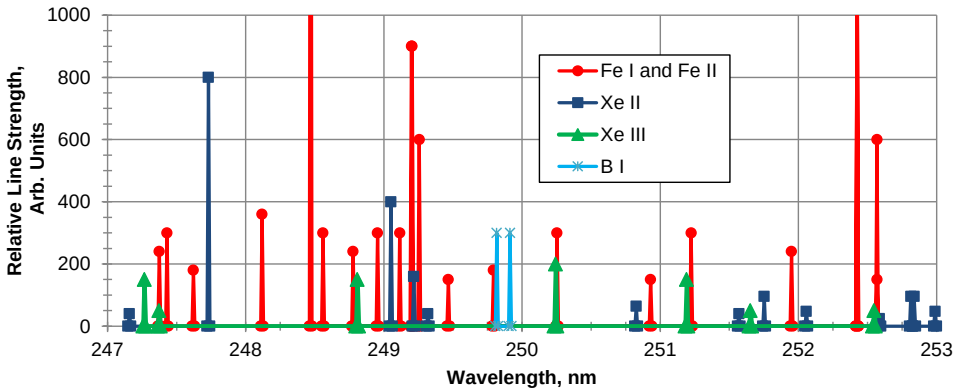

a. Relative transition strengths of iron, xenon, and boron in the region of interest.

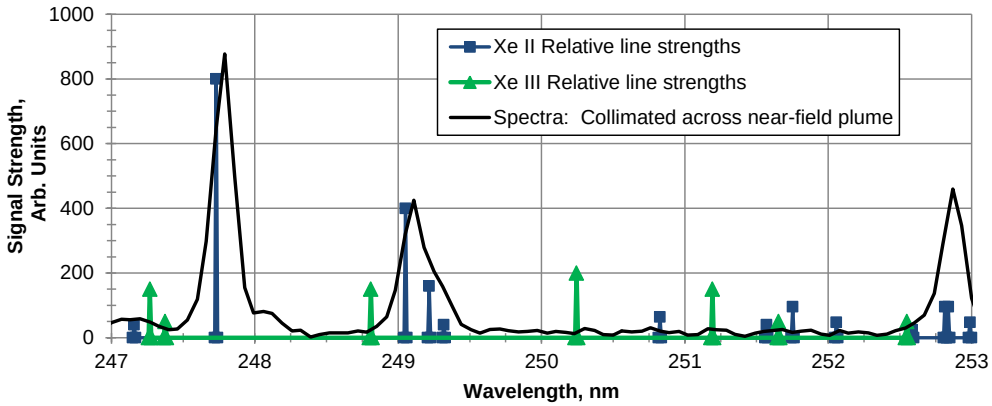

b. Correlation of typical cross-plume spectra with xenon transitions. Note that there are no significant peaks away from these transitions

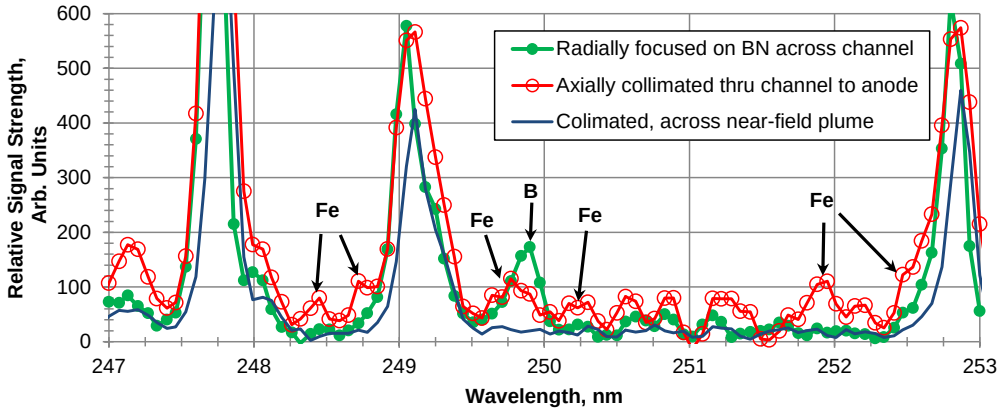

c. Overlay of emission spectra showing that Fe does not appear to be present in cross-channel or wall-focused probe data.

Figure 2 Comparison of typical and axial optical emission spectra from 247 nm to 253 nm .

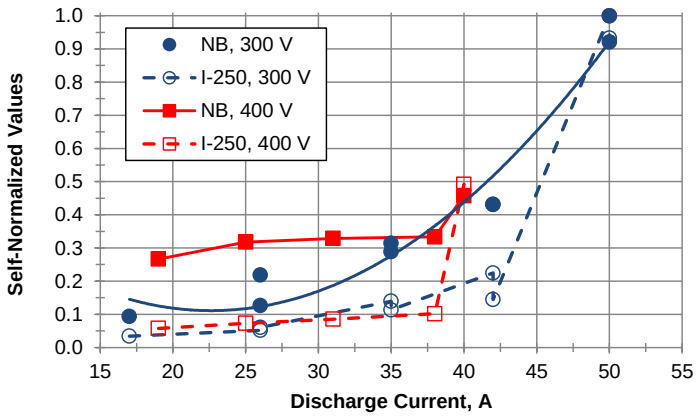

Figure 3 Comparison of corrected, $I_{B,\ 250\ nm}$, and normalized, N_B, values.

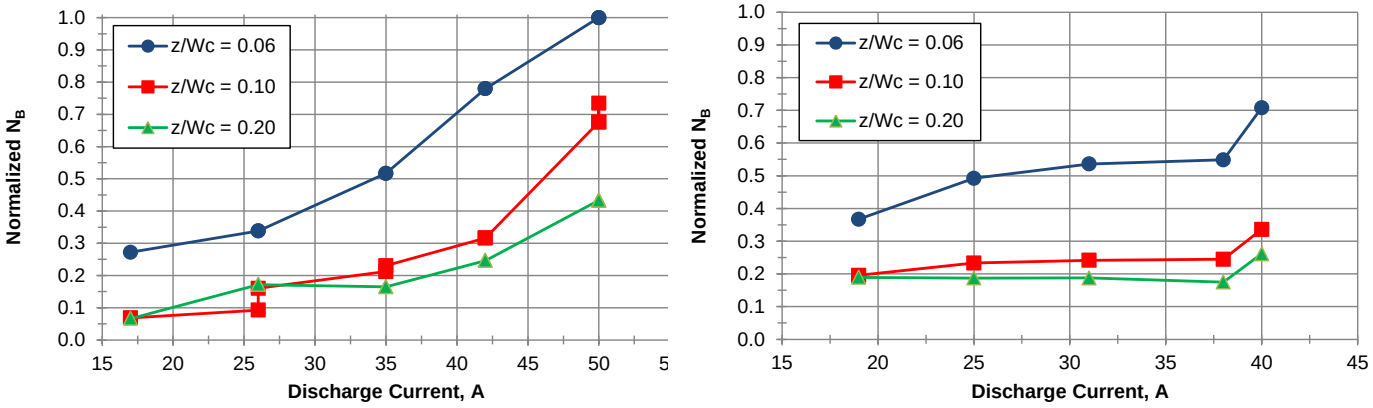

a. Vd = 300 V **b. Vd = 400 V**

Figure 4 Comparison of N_B trends for three axial locations along the inner wall for V_D = 300 V and V_D = 400 V.

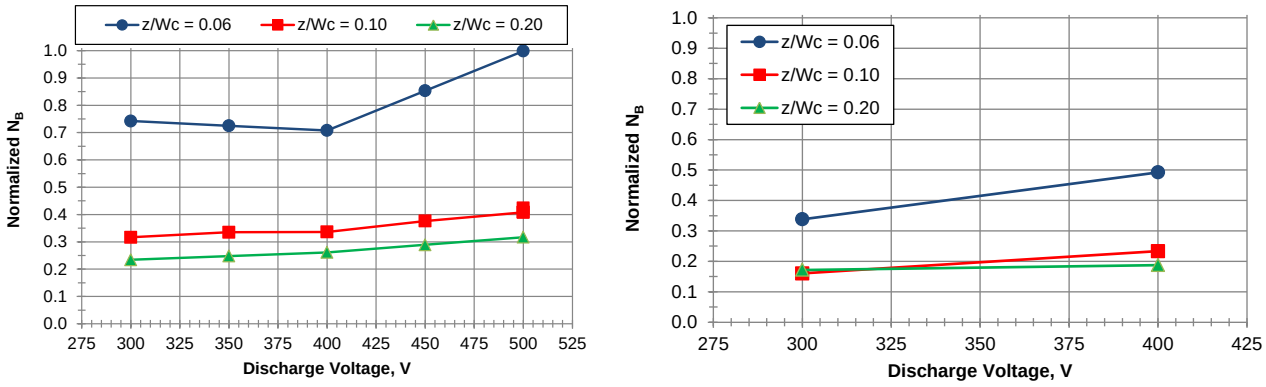

a. Jd = 40 A **b. Jd = 25 A**

Figure 5 Comparison of N_B trends for three axial locations along the inner wall for J_D = 40 A and J_D = 25 A.

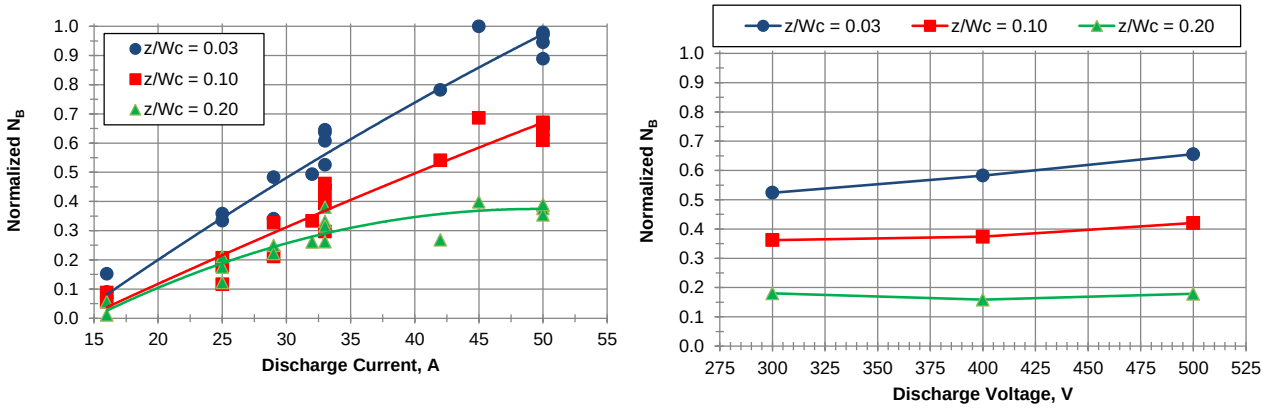

a. Vd = 300 V **b. Jd = 40 A**

Figure 6 Comparison of N_B trends for three axial locations along the outer wall for V_D = 300 V and J_D = 40 A.

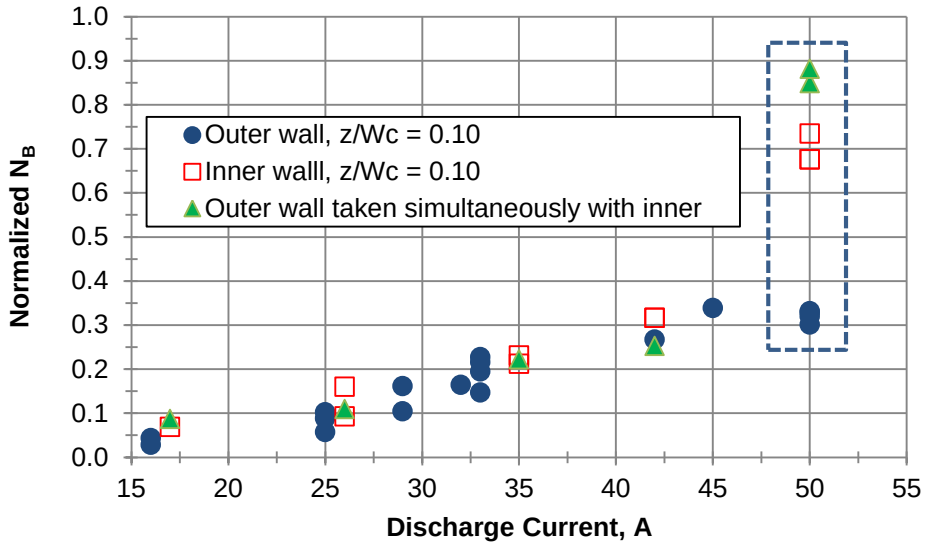

Figure 7 Comparison of inner wall and outer wall N_B trends at the z/W_C = 0.10 location for V_D = 300 V. Note that the outer wall data taken previously to and simultaneously with the inner wall data agree except at the J_D = 50 A condition.

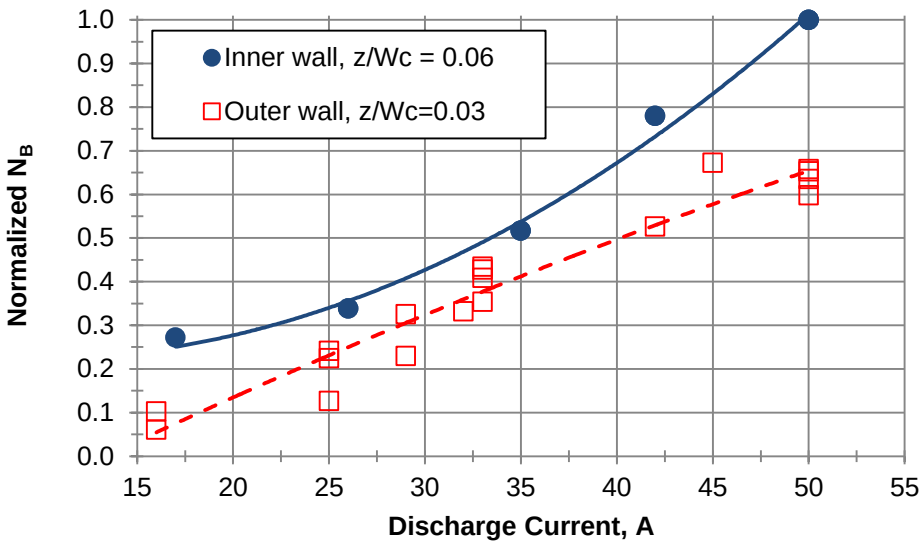

Figure 8 Comparison of inner wall and outer wall N_B trends at the z/W_C = 0.06 (inner wall) and 0.03 (outer wall) locations for V_D = 300 V. Trendlines are for illustrative purposes only.